A preliminary diffusional kurtosis imaging study of Parkinson disease: comparison with conventional diffusion tensor imaging

**Koji Kamagata · Hiroyuki Tomiyama · Taku Hatano · Yumiko Motoi · Osamu Abe ·
Keigo Shimoji · Kouhei Kamiya · Michimasa Suzuki · Masaaki Hori · Mariko Yoshida ·
Nobutaka Hattori · Shigeki Aoki**

Abstract

Introduction Diffusional kurtosis imaging (DKI) is a more sensitive technique than conventional diffusion tensor imaging (DTI) for assessing tissue microstructure. In particular, it quantifies the microstructural integrity of white matter, even in the presence of crossing fibers. The aim of this preliminary study was to compare how DKI and DTI show white matter alterations in Parkinson disease (PD).

Methods DKI scans were obtained with a 3-T magnetic resonance imager from 12 patients with PD and 10 healthy controls matched by age and sex. Tract-based spatial statistics were used to compare the mean kurtosis (MK), mean diffusivity (MD), and fractional anisotropy (FA) maps of the PD patient group and the control group. In addition, a region-of-interest analysis was performed for the area of the posterior corona radiata and superior longitudinal fasciculus (SLF) fiber crossing.

Results FA values in the frontal white matter were significantly lower in PD patients than in healthy controls. Reductions in MK occurred more extensively throughout the brain: in addition to frontal white matter, MK was lower in the parietal,

occipital, and right temporal white matter. The MK value of the area of the posterior corona radiata and SLF fiber crossing was also lower in the PD group.

Conclusion DKI detects changes in the cerebral white matter of PD patients more sensitively than conventional DTI. In addition, DKI is useful for evaluating crossing fibers. By providing a sensitive index of brain pathology in PD, DKI may enable improved monitoring of disease progression.

Keywords Diffusional kurtosis imaging · Diffusion tensor imaging · Parkinson disease · Tract-based spatial statistics

Abbreviations

DTI	Diffusion tensor imaging
DKI	Diffusional kurtosis imaging
FA	Fractional anisotropy
MD	Mean diffusivity
MK	Mean kurtosis
PD	Parkinson disease
ROI	Region of interest
SLF	Superior longitudinal fasciculus
TBSS	Tract-based spatial statistics

K. Kamagata (✉) · K. Kamiya · M. Suzuki · M. Hori ·
M. Yoshida · S. Aoki
Department of Radiology, Juntendo University School of Medicine,
2-1-1 Hongo, Bunkyo-ku, Tokyo 113-8421, Japan
e-mail: kkamagat@juntendo.ac.jp

H. Tomiyama · T. Hatano · Y. Motoi · N. Hattori
Department of Neurology, Juntendo University School of Medicine,
Tokyo, Japan

O. Abe
Department of Radiology, Nihon University School of Medicine,
Tokyo, Japan

K. Shimoji
Department of Radiology, National Center of Neurology and
Psychiatry Hospital, Tokyo, Japan

Introduction

Parkinson disease (PD) is a chronic, progressive, and degenerative neurological disorder defined by its motor symptoms (akinesia, resting tremor, and rigidity) and numerous nonmotor symptoms (such as cognitive impairment, depression, and olfactory dysfunction) [1]. In PD, these motor and nonmotor symptoms reflect the widespread progression of underlying pathologies, which include α-synuclein-immunoreactive inclusions in the cytoplasm of neurons

(Lewy bodies) and within neuronal processes (Lewy neurites), loss of dopaminergic projections from the substantia nigra to the striatum, and progressive loss of cholinergic and mono-aminergic cortical projections from the nucleus basalis of Meynert [2–6].

Conventional magnetic resonance imaging (MRI) has been unsuccessful for discerning these pathophysiologic changes in PD; because the results are usually nonspecific, the role of MRI is confined to excluding secondary causes of parkinsonism such as vascular lesions. By contrast, diffusion tensor imaging (DTI) in PD provides quantitative measures of microstructural integrity and organization in vivo and is thus more suitable for detecting subtle alterations not evident with conventional MRI [7–12]. Diffusional abnormalities of frontal white matter have been consistently observed in DTI studies of PD patients [9, 13–16]. DTI with region-of-interest (ROI) analyses has revealed changes in fractional anisotropy (FA) in the frontal lobes of PD patients relative to controls [13]. Karagulle et al. used voxel-based analysis in conjunction with DTI to compare PD patients to controls and observed decreased FA bilaterally in the frontal lobes, including the supplementary and presupplementary motor areas [9]. Similarly, Zhan et al. found reduced FA in the frontal lobes, including the precentral gyrus and supplementary motor areas [14].

In traditional DTI theory, a perfect Gaussian distribution is assumed for the movement of water molecules [17]. However, water in biological structures often shows non-Gaussian diffusion because it is restricted by diffusion barriers such as cell membranes and organelles. Therefore, the assumption of Gaussian water diffusion may be inappropriate in biological structures. Diffusional kurtosis imaging (DKI) has been proposed as a natural extension of DTI that enables the quantification of non-Gaussian diffusion [18–21]. In addition to conventional DTI metrics such as mean diffusivity (MD) and FA, an additional metric related to non-Gaussian water diffusion called mean kurtosis (MK) is obtained in DKI, whereby a higher MK value suggests a more hindered and restricted diffusion environment [22]. In contrast to conventional DTI metrics, MK is not limited to anisotropic environments; hence, it especially permits quantification of the microstructural integrity of white matter, even in the presence of crossing fibers.

These properties of MK have led to its application to the brains of patients with PD. Wang et al. reported increased MK in the basal ganglia and substantia nigra using ROI analysis [23]. They found that MK in the ipsilateral substantia nigra showed the best diagnostic performance relative to the conventional diffusion tensor parameter. We also found that FA and MK were reduced in the cingulate fiber tracts in PD patients relative to controls and that MK in the anterior cingulum showed the best diagnostic performance [24]. However, whole-brain voxel-based DKI analyses have yet to be performed in PD patients. Voxel-based analysis is a technique that can identify the changes of diffusion tensor parameter in

any part of the whole brain without a prior hypothesis, unlike ROI analysis.

Here, we expanded on our previous work and conducted whole-brain DKI analyses of PD patients and controls by using tract-based spatial statistics (TBSS) [25] implemented in the FMRIB Software Library 4.1.5 (FSL, Oxford Centre for Functional MRI of the Brain, UK; www.fmrib.ox.ac.uk/fsl) and we compared the data with those obtained with conventional DTI parameters. Thus, the aims of this preliminary study were to investigate how white matter is altered in PD as measured with DKI and to compare the results to those previously demonstrated with DTI.

Materials and methods

Subjects

The participants were PD patients who had been diagnosed by neurologists specializing in movement disorders. Each participant fulfilled the UK Parkinson's Disease Society Brain Bank criteria and was found to be at stage I, II, or III on the Hoehn and Yahr scale. All PD patients were taking levodopa and a dopamine decarboxylase inhibitor (benserazide or carbidopa) at the time of the MR imaging and clinical examination. Eighteen months or more after scanning, all patients remained free of atypical parkinsonism and continued to respond satisfactorily to antiparkinsonian therapy. Ten age- and gender-matched control subjects were voluntarily recruited. None of the control subjects had any history of neurologic or psychiatric disorders or showed any abnormal signal in structural MR imaging.

This study was approved by the ethical committee of Juntendo Hospital, Juntendo University, and informed consent was obtained from all the participants before evaluation. The demographic characteristics of the participants are shown in Table 1.

MR imaging

All MR images were obtained by using a 3.0-T system (Achieva; Philips Healthcare, Best, the Netherlands) equipped with an eight-channel head coil for sensitivity-encoding parallel imaging. Regular structural images such as T1-weighted spin-echo images, T2-weighted turbo spin-echo images, and fluid-attenuated inversion recovery images were obtained before acquiring diffusion tensor and kurtosis images.

DKI data were acquired with a spin-echo EPI sequence along 20 isotropic diffusion gradient directions. For each direction, DKI images were acquired with three values of b (0, 1,000, and 2,000 s/mm^2). The sequence parameters were as follows: image orientation, axial; repetition time (TR), 7,041 ms; echo time (TE), 70 ms; diffusion gradient pulse

Table 1 Demographic characteristics of subjects

	Normal controls (n=10)	PD patients (n=12)	P value
Sex, male/female	5:5	6:6	0.42
Age in years, mean (SD)	67.6 (10.1)	65.4 (10.0)	0.82
Disease duration in years, mean (SD)	NA	7.1 (4.5)	NA
Hoehn–Yahr stage (SD)	0	2.6 (0.8)	NA
Levodopa dosage, mg/day, median (SD)	0	322.7 (194.1)	NA

PD Parkinson disease, *SD* standard deviation, *NA* not applicable

duration (δ), 13.3 ms; diffusion gradient separation (Δ), 45.3 ms; number of excitations (NEX), 1; field of view, 240 mm; matrix, 80×80; slice thickness, 3 mm; number of slices, 50; and imaging time, 6 min 26 s.

Diffusion tensor and kurtosis analyses were performed on an independent Windows PC by using the free software dTV II FZRx and Volume-One 1.81 (http://www.volume-one.org), developed by Masutani et al. (The University of Tokyo; diffusion tensor visualizer available at http://www.ut-radiology.umin.jp/people/masutani/dTV.htm) [7, 26, 27]. First, FA and MD maps based on the conventional mono-exponential model were calculated. Because the kurtosis data was generated using multiple values of b, the FA and MD could be calculated by using part of the diffusion kurtosis data. Next, mean DK maps were obtained (Fig. 1). The details of the procedure for calculating the maps were as previously described [19, 22, 28]. As described in previous papers [19, 22], the DK value for a single direction is determined by acquiring data at three or more b values (including b=0) and fitting them to Eq. (1):

$$\ln[S(b)] = \ln[S(0)] - b \times \text{Dapp} + 1/6 \times b2 \times \text{D2app} \times \text{Kapp} \tag{1}$$

where Dapp is the MD for the given direction and Kapp is the apparent kurtosis coefficient, which is dimensionless.

DTI/DKI image processing with TBSS

Voxel-based analysis of the DTI/DKI data was performed with TBSS [21] implemented in FMRIB Software Library 4.1.5 (FSL, Oxford Centre for Functional MRI of the Brain, UK; www.fmrib.ox.ac.uk/fsl). We corrected for distortions due to eddy currents by affine intrasubject registration to the respective individual $b0$ image by means of the EDDYCORRECT procedure implemented in FSL [29]. FA and MD maps for all subjects were calculated by fitting a tensor model to each voxel of the raw diffusion data, using the tool DTIFIT. Nonbrain structures were eliminated by using the brain extraction tool. FA maps of all subjects were aligned to standard Montreal Neurological Institute (MNI152) space

by using the nonlinear registration tool FNIRT. Next, the mean FA image was generated and thinned to create the mean FA skeleton, which represented the centers of all tracts common to the groups. The mean FA skeleton was thresholded to FA >0.20 to include the major white matter pathways but exclude peripheral tracts and gray matter. The aligned FA map of each participant was then projected onto this skeleton by assigning to each point on the skeleton the maximum FA in a plane perpendicular to the local skeleton structure. The resulting skeletons were fed into voxel-wise statistics. By applying the original nonlinear registration of the FA of each subject to the standard space, the MD map was also projected onto the mean FA skeleton. The MD data were used to calculate voxel-wise statistics as well. Voxel-wise statistics of the skeletonized FA data were analyzed with Randomise (part of FSL) to test for group differences between the patient and control groups. This program performed permutation-based testing with 5,000 permutations and statistical inference by using threshold-free cluster enhancement (TFCE) [22] with a threshold of P<0.05, corrected for multiple comparisons (family-wise error). Randomise was also used to examine the relationship between FA/MD/MK and disease duration, Hoehn–Yahr stage, and levodopa dosage in the PD patient group with multiple linear regression analysis (P<0.05, corrected for gender and age at the time of MRI). The anatomical locations of regions with significant group differences in FA and MD on the white matter skeleton were identified with a white matter atlas [23].

Analysis of crossing fibers

The superior longitudinal fasciculus (SLF) contains a relatively large number of voxels with multiple fiber orientations due to the crossing of the corona radiata, laterally projecting fibers of the corpus callosum, or both [30]. ROI analysis was performed for the area of the posterior corona radiata and SLF fiber crossing.

On the color maps, red, green, and blue were assigned to the left–right, antero-posterior, and cranio-caudal directions, respectively. The corona radiata are easily identified in blue owing to their predominantly cranio-caudal direction (Fig. 1a). Fibers of the SLF are identified in green owing to
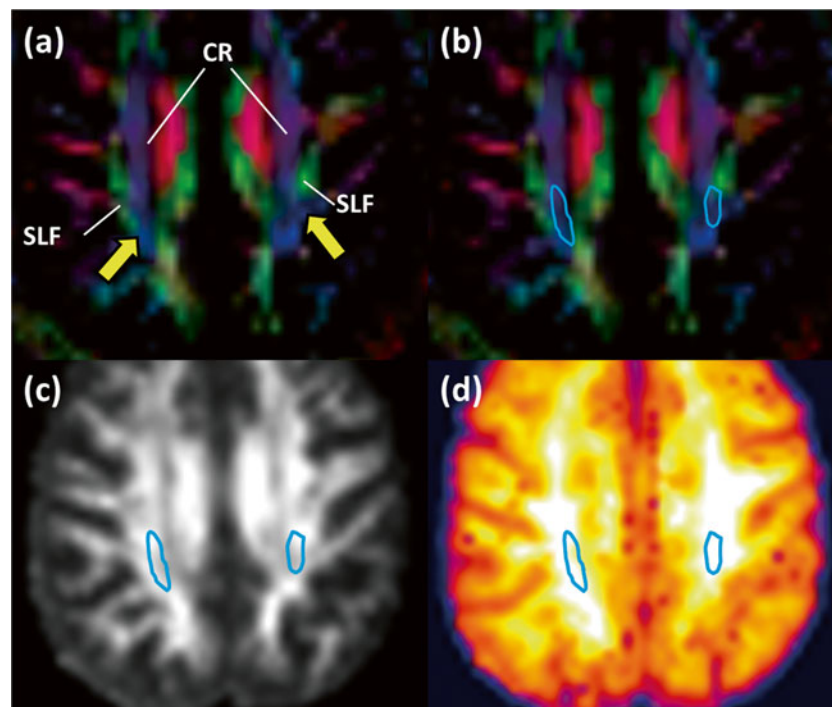
Fig. 1 Procedure used to draw regions of interest (ROI) on the area of the posterior corona radiata and crossing fibers of the superior longitudinal fasciculus (SLF). Axial color-coded fractional anisotropy (FA) maps (**a**, **b**) and an FA map (**c**) and corresponding and mean kurtosis (MK) map (**d**) depicting the superior longitudinal fasciculus (SLF) and posterior corona radiata (CR) are shown. **a** The CR were easily identified in *blue* on the color map owing to their predominantly cranio-caudal direction. The SLF was also identified in *green* on the color map owing to its predominantly antero-posterior orientation. In the area of the posterior corona radiata and SLF fiber crossing, *blue* (corona radiata) and *green* (SLF) are intermingled and the color becomes ambiguous (marked by *yellow arrows*). **b** On the color map, we identified the axial slice where the area of the posterior corona radiata and SLF fiber crossing became the largest. In this slice, we drew the ROI manually on the area of the posterior corona radiata and SLF fiber crossing (*blue line*). **c**, **d** We applied this ROI to the FA (**c**) and MK (**d**) maps of the same slice

their predominantly antero-posterior orientation (Fig. 1a). In the area of the posterior corona radiata and SLF fiber crossing, blue (corona radiata) and green (SLF) are intermingled and the color becomes ambiguous (Fig. 1a).

The following method was used to draw an ROI. First, on the color map, we identified the axial slice where the area of the posterior corona radiata and SLF fiber crossing was the largest (Fig. 1a). Second, in this slice, we drew the ROI manually on the area of the posterior corona radiata and SLF crossing fibers (Fig. 1b). We applied this ROI to FA and MK maps of the same slice (Fig. 1c, d). Both investigators agreed a priori upon the common method described above. All ROIs were drawn by individuals blind to the patient or control status.

Statistical analysis

All statistical analyses were performed with the Statistical Package for the Social Sciences for Windows, Release 20.0 (SPSS, Chicago, IL). Statistical analysis of demographic and clinical data was conducted with Student's t test for continuous variables and the χ^2 test for categorical data. The criterion of statistical significance was set to $P<0.05$. Student's t test was used to compare the averaged values of MD, FA, and MK for the area of the posterior corona radiata and SLF fiber crossing between PD patients and healthy controls. A Bonferroni correction was applied to the number of comparisons ($n=3$: [MD, FA, MK], setting the level of significance at $P<0.05/3=0.016$). Interrater reliability was assessed by using Pearson's correlation coefficient.

Results

Demographic and clinical features

Age ($P=0.82$, Student's t test) and sex distribution ($P=0.42$, χ^2) did not differ between PD patients and healthy controls (Table 1).

White matter alteration assessed with TBSS

FA values in the frontal white matter, part of the genu of the corpus callosum, and part of the parietal white matter were significantly lower in PD patients than in healthy controls. The affected white matter tracts included the anterior part of the

inferior fronto-occipital fasciculus (IFOF), anterior SLF, and anterior and superior corona radiata (i.e., the frontal white matter); in part of the posterior SLF and in part of the genu and body of the corpus callosum, FA values were significantly lower in controls than in PD patients (Fig. 2a).

Reductions in MK were seen more extensively throughout the brain: in addition to the frontal white matter, reduced MK was seen in the parietal, occipital, and right temporal white matter. The affected white matter tracts included the SLF and inferior longitudinal fasciculus; the IFOF; the uncinate fasciculus; and the anterior, posterior, and superior corona radiata (Fig. 2b). MD values were not significantly different in the cerebral white matter of PD patients compared with control subjects.

Analysis of crossing fibers

Compared with the area of parietal white matter in which FA was reduced, the MK reduction area was wider in range and included the area of the posterior corona radiata and SLF fiber crossing. In contrast to FA, MK is not limited to anisotropic environments; hence, it uniquely permits quantification of the microstructural integrity of white matter in the presence of crossing fibers. We hypothesized that the area of the posterior corona radiata and SLF fiber crossing influenced our TBSS results. We therefore compared diffusion abnormalities in the area of the posterior corona radiata and SLF fiber crossing in PD patients and normal controls by using an ROI analysis.

Reproducibility was expressed in terms of the interrater correlation coefficient; the coefficient in the posterior corona radiata crossing fibers of the SLF was 0.89 for the MD

analysis. 0.84 for the FA analysis, and 0.95 for the MK analysis. Therefore, averaged values were used for subsequent statistical analyses.

FA and MD values were not significantly altered in the area of the posterior corona radiata and SLF fiber crossing in the PD group compared with the control group (MD: $P=0.36$, FA: $P=0.95$) (Table 2). Only MK values were reduced in the PD group compared with the control group (MK: $P=0.001$) (Table 2).

Discussion

Three findings were confirmed in this study. First, we demonstrated that FA values in the frontal white matter (anterior part of the IFOF, anterior SLF, and anterior and superior corona radiata), part of the genu and body of the corpus callosum, and part of the parietal white matter (in part of the posterior SLF) were significantly lower in PD patients than in healthy controls. Second, reductions in MK values occurred across a more extensive area than FA reduction: in addition to the frontal white matter, reduced MK values were seen in the parietal, occipital, and right temporal white matter. Third, the MK value of the area of the posterior corona radiata and SLF fiber crossing was reduced in the PD group compared with the control group. Although previous DKI studies of the basal ganglia and substantia nigra by Wang et al. [23] and of the cingulate fiber tracts by our group [24] have revealed changes in diffusion metrics specific to PD patients, to the best of our knowledge, the present study is the first to evaluate white matter by using whole-brain DKI analysis in PD patients.
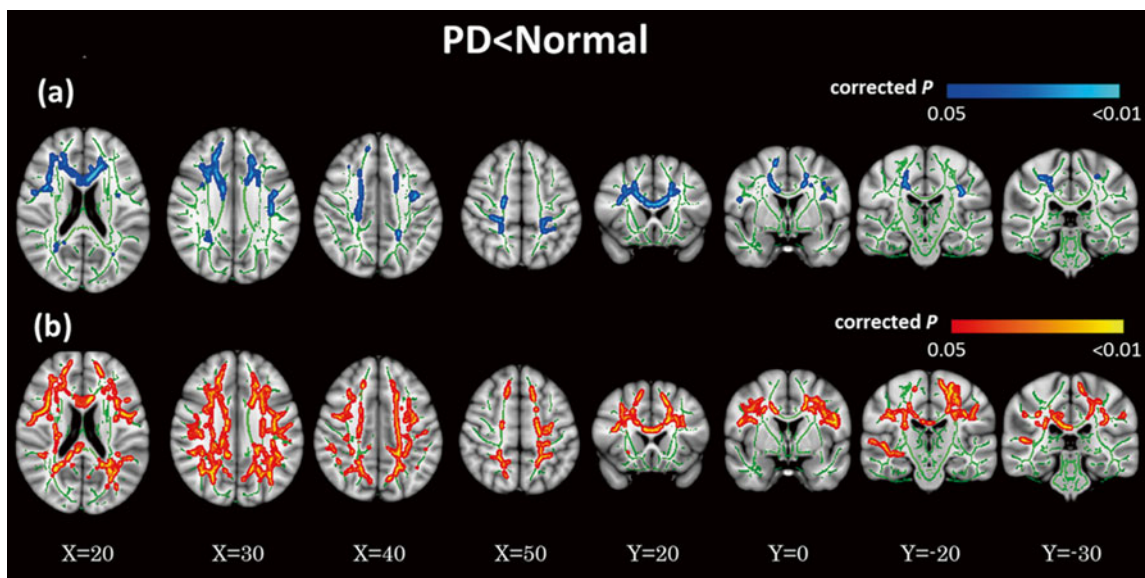

Fig. 2 Comparison of DTI and DKI metrics between PD patients and controls. TBSS maps of decreased FA (**a**) and decreased MK (**b**) in PD patients compared with age-matched healthy subjects shown in neurological convention. In the TBSS maps, the FA skeleton with FA >0.2 is shown in *green*, and voxels in which the one-sided permutation-corrected P was <0.05 are marked in *blue* (FA) or *red* (MK)

Table 2 Comparison of DT/DK parameters in the area of the posterior corona radiata and SLF fiber crossing

	CN	PD	PD − N (%)	P value
Area of the posterior corona radiata and SLF fiber crossing				
MK	1.15±0.06	1.04±0.06	−9.5	0.001[a]
FA	0.32±0.03	0.32±0.08	−2.8	0.95
MD	0.71±0.02	0.73±0.04	+2.1	0.36

Values are means ± SD. FA and MK are dimensionless. Mean diffusivity values are given in 1,000 mm^2/s. PD − N = (PD − N) / N × 100

CN healthy controls, *PD* Parkinson disease, *MK* mean kurtosis, *FA* fractional anisotropy, *MD* mean diffusivity

[a] Significant difference between groups

The reduced FA values in the frontal lobe of PD patients agree with the results of previous studies [9, 13–15]. According to the staging system proposed by Braak et al. [2, 4], neuropathological stages are divided into six subgroups depending on where Lewy bodies are deposited. In stages 1 and 2, Lewy-related inclusion bodies remain confined to the medulla oblongata and olfactory bulb. In stages 3 and 4, the substantia nigra and other nuclei of the midbrain and basal forebrain are the focus of initially subtle and later severe changes. In end stages 5 and 6, the pathological process encroaches upon the cerebral cortex. The deposition of Lewy bodies in the prefrontal area is classified as stage 5—a relatively early stage for the neocortex. Pathological changes in white matter in the form of Lewy neurites or pale neurites, which accumulate in brainstem axons and later spread to the cerebral white matter, are also found in parallel with Lewy bodies in PD [2, 4]. These accumulated Lewy pathologies may alter the axonal structure. The decrease in FA may reflect neuronal loss and reduced anisotropy due to the deposition of axonal Lewy neurites or pale neurites.

Currently, mainly the end phase of the pathologic process of PD can be detected clinically [2, 4]. In Braak staging, autopsy material from patients who manifest clinical findings consistent with PD can be assigned to one of three subgroups (stages 4–6) depending on the locations of Lewy deposits. In stage 6, Lewy-related pathology reaches the entire cerebrum; therefore, the extensive area across which MK was reduced may reflect white matter alteration caused by Lewy-related pathologies such as Lewy neurites or pale neurites.

Although traditional DTI assumes that water molecules display Gaussian diffusion in a hindered and unrestricted environment, in biological structures, they are restricted by cell membranes or organelles and thus often display non-Gaussian diffusion. Therefore, the sensitivity of DTI is limited by the diffusional and microstructural properties of biological structures [31]. Because kurtosis is a measure of the deviation of the diffusion profile from a Gaussian distribution, DKI quantifies the degree of diffusional non-Gaussianity or tissue complexity. Therefore, DKI would appear adequate for analyzing the structure of the human brain [31]. Our results suggest that the assessment of diffusional non-Gaussianity by using DKI may supply more sensitive metrics of changes in tissue microstructure than does traditional DTI.

DKI is also potentially useful for evaluating crossing fibers [32], whereas DTI metrics such as FA and MD in white matter are influenced by the presence of crossing fibers [33–35]. The adverse effects of crossing fibers on the interpretation of DTI metrics have been previously demonstrated [36, 37]. If two fiber populations are present within a voxel (crossing fiber), the shape of the diffusion tensor becomes more planar. Therefore, FA and MD values are lower in areas where fibers cross because of the lower directionality of diffusion on the voxel scale [36, 37]. As a result, the FA value of a voxel with intact crossing fibers can be similar to that of a voxel with a degenerating area with noncrossing fibers [30]. In our TBSS results, the area of MK reduction includes that of the posterior corona radiata and SLF crossing fibers, whereas no change in FA was observed in this area. Furthermore, a significant MK reduction in this area was also detected by ROI analysis, whereas no such change of MD or FA occurred in this area, confirming the robustness of our results. That DKI can identify areas of fiber crossing may be one reason why MK is sensitive to changes in cerebral white matter.

Our study has a number of limitations. First, because the PD diagnoses were not histopathologically confirmed, the possibility of misdiagnosis remains. However, the validity of the diagnoses is strengthened by the observation that, after being followed for 18 months, all patients continued to respond satisfactorily to antiparkinsonian therapy and remained free of atypical parkinsonisms. Second, the small size of our samples may have limited the comparison of disease severity and DT/DK parameters. Third, the ROIs on the area of the posterior corona radiata and SLF fiber crossing were drawn manually, and the reproducibility of measurements was unclear. However, all ROIs were drawn by two of the authors, rater bias was prevented by blinding, and the interclass correlation coefficients were 0.84–0.95.

Conclusion

DKI can detect cerebral white matter alteration in PD patients more sensitively than can conventional DTI. By providing a potentially more sensitive index of brain pathology in PD, DKI may enable improved monitoring of disease progression and more effective treatment planning.

References

1. de Lau LM, Breteler MM (2006) Epidemiology of Parkinson's disease. Lancet Neurol 5(6):525–535. doi:10.1016/S1474-4422(06)70471-9

2. Braak H, Del Tredici K (2008) Invited article: nervous system pathology in sporadic Parkinson disease. Neurology 70(20):1916–1925. doi:10.1212/01.wnl.0000312279.49272.9f

3. Braak H, Del Tredici K, Bratzke H, Hamm-Clement J, Sandmann-Keil D, Rub U (2002) Staging of the intracerebral inclusion body pathology associated with idiopathic Parkinson's disease (preclinical and clinical stages). J Neurol 249(Suppl 3):III/1–III/5

4. Braak H, Del Tredici K, Rub U, de Vos RA, Jansen Steur EN, Braak E (2003) Staging of brain pathology related to sporadic Parkinson's disease. Neurobiol Aging 24(2):197–211

5. Braak H, Ghebremedhin E, Rub U, Bratzke H, Del Tredici K (2004) Stages in the development of Parkinson's disease-related pathology. Cell Tissue Res 318(1):121–134. doi:10.1007/s00441-004-0956-9

6. Braak H, Muller CM, Rub U, Ackermann H, Bratzke H, de Vos RA, Del Tredici K (2006) Pathology associated with sporadic Parkinson's disease—where does it end? J Neural Transm Suppl 70:89–97

7. Kamagata K, Motoi Y, Abe O, Shimoji K, Hori M, Nakanishi A, Sano T, Kuwatsuru R, Aoki S, Hattori N (2012) White matter alteration of the cingulum in Parkinson disease with and without dementia: evaluation by diffusion tensor tract-specific analysis. AJNR Am J Neuroradiol 33(5):890–895. doi:10.3174/ajnr.A2860

8. Kamagata K, Motoi Y, Hori M, Suzuki M, Nakanishi A, Shimoji K, Kyougoku S, Kuwatsuru R, Sasai K, Abe O, Mizuno Y, Aoki S, Hattori N (2011) Posterior hypoperfusion in Parkinson's disease with and without dementia measured with arterial spin labeling MRI. J Magn Reson Imaging JMRI 33(4):803–807. doi:10.1002/jmri.22515

9. Karagulle Kendi AT, Lehericy S, Luciana M, Ugurbil K, Tuite P (2008) Altered diffusion in the frontal lobe in Parkinson disease. AJNR Am J Neuroradiol 29(3):501–505. doi:10.3174/ajnr.A0850

10. Lee JE, Park HJ, Park B, Song SK, Sohn YH, Lee JD, Lee PH (2010) A comparative analysis of cognitive profiles and white-matter alterations using voxel-based diffusion tensor imaging between patients with Parkinson's disease dementia and dementia with Lewy bodies. J Neurol Neurosurg Psychiatry 81(3):320–326. doi:10.1136/jnnp.2009.184747

11. Vaillancourt DE, Spraker MB, Prodoehl J, Abraham I, Corcos DM, Zhou XJ, Comella CL, Little DM (2009) High-resolution diffusion tensor imaging in the substantia nigra of de novo Parkinson disease. Neurology 72(16):1378–1384. doi:10.1212/01.wnl.0000340982.01727.6e

12. Hattori T, Orimo S, Aoki S, Ito K, Abe O, Amano A, Sato R, Sakai K, Mizusawa H (2012) Cognitive status correlates with white matter alteration in Parkinson's disease. Hum Brain Mapp 33(3):727–739. doi:10.1002/hbm.21245

13. Matsui H, Nishinaka K, Oda M, Niikawa H, Kubori T, Udaka F (2007) Dementia in Parkinson's disease: diffusion tensor imaging. Acta Neurol Scand 116(3):177–181. doi:10.1111/j.1600-0404.2007.00838.x

14. Zhan W, Kang GA, Glass GA, Zhang Y, Shirley C, Millin R, Possin KL, Nezamzadeh M, Weiner MW, Marks WJ Jr, Schuff N (2012) Regional alterations of brain microstructure in Parkinson's disease using diffusion tensor imaging. Mov Disord Off J Mov Disord Soc 27(1):90–97. doi:10.1002/mds.23917

15. Zhang K, Yu C, Zhang Y, Wu X, Zhu C, Chan P, Li K (2011) Voxel-based analysis of diffusion tensor indices in the brain in patients with Parkinson's disease. Eur J Radiol 77(2):269–273. doi:10.1016/j.ejrad.2009.07.032

16. Haller S, Badoud S, Nguyen D, Garibotto V, Lovblad KO, Burkhard PR (2012) Individual detection of patients with Parkinson disease using support vector machine analysis of diffusion tensor imaging data: initial results. AJNR Am J Neuroradiol 33(11):2123–2128. doi:10.3174/ajnr.A3126

17. Basser PJ, Jones DK (2002) Diffusion-tensor MRI: theory, experimental design and data analysis—a technical review. NMR Biomed 15(7–8):456–467. doi:10.1002/nbm.783

18. Hui ES, Cheung MM, Qi L, Wu EX (2008) Towards better MR characterization of neural tissues using directional diffusion kurtosis analysis. Neuroimage 42(1):122–134. doi:10.1016/j.neuroimage.2008.04.237

19. Jensen JH, Helpern JA, Ramani A, Lu H, Kaczynski K (2005) Diffusional kurtosis imaging: the quantification of non-Gaussian water diffusion by means of magnetic resonance imaging. Magn Reson Med Off J Soc Magn Reson Med Soc Magn Reson Med 53(6):1432–1440. doi:10.1002/mrm.20508

20. Lu H, Jensen JH, Ramani A, Helpern JA (2006) Three-dimensional characterization of non-Gaussian water diffusion in humans using diffusion kurtosis imaging. NMR Biomed 19(2):236–247. doi:10.1002/nbm.1020

21. Jensen JH HJ (2003a) Quantifying non-Gaussian water diffusion by means of pulsed-field-gradient MRI. Presented at the International Society for Magnetic Resonance in Medicine annual meeting, Toronto, Canada 11:2154

22. Jensen JH, Helpern JA (2010) MRI quantification of non-Gaussian water diffusion by kurtosis analysis. NMR Biomed 23(7):698–710. doi:10.1002/nbm.1518

23. Wang JJ, Lin WY, Lu CS, Weng YH, Ng SH, Wang CH, Liu HL, Hsieh RH, Wan YL, Wai YY (2011) Parkinson disease: diagnostic utility of diffusion kurtosis imaging. Radiology 261(1):210–217. doi:10.1148/radiol.11102277

24. Kamagata K, Tomiyama H, Motoi Y, Kano M, Abe O, Ito K, Shimoji K, Suzuki M, Hori M, Nakanishi A, Kuwatsuru R, Sasai K, Aoki S, Hattori N (2013) Diffusional kurtosis imaging of cingulate fibers in Parkinson disease: comparison with conventional diffusion tensor imaging. Magn Reson Imaging 31(9):1501–1506. doi:10.1016/j.mri.2013.06.009

25. Smith SM, Jenkinson M, Johansen-Berg H, Rueckert D, Nichols TE, Mackay CE, Watkins KE, Ciccarelli O, Cader MZ, Matthews PM, Behrens TE (2006) Tract-based spatial statistics: voxelwise analysis of multi-subject diffusion data. Neuroimage 31(4):1487–1505. doi:10.1016/j.neuroimage.2006.02.024

26. Kubicki M, Westin CF, Maier SE, Frumin M, Nestor PG, Salisbury DF, Kikinis R, Jolesz FA, McCarley RW, Shenton ME (2002) Uncinate fasciculus findings in schizophrenia: a magnetic resonance diffusion tensor imaging study. AJ Psychiatry 159(5):813–820

27. Kunimatsu A, Aoki S, Masutani Y, Abe O, Mori H, Ohtomo K (2003) Three-dimensional white matter tractography by diffusion tensor imaging in ischaemic stroke involving the corticospinal tract. Neuroradiology 45(8):532–535. doi:10.1007/s00234-003-0974-4

28. Hori M, Fukunaga I, Masutani Y, Nakanishi A, Shimoji K, Kamagata K, Asahi K, Hamasaki N, Suzuki Y, Aoki S (2012) New diffusion metrics for spondylotic myelopathy at an early clinical stage. Eur Radiol 22(8):1797–1802. doi:10.1007/s00330-012-2410-9

29. Jenkinson M, Bannister P, Brady M, Smith S (2002) Improved optimization for the robust and accurate linear registration and motion correction of brain images. Neuroimage 17(2):825–841

30. Reijmer YD, Leemans A, Heringa SM, Wielaard I, Jeurissen B, Koek HL, Biessels GJ (2012) Improved sensitivity to cerebral white matter abnormalities in Alzheimer's disease with spherical deconvolution based tractography. PLoS One 7(8):e44074. doi:10.1371/journal.pone.0044074

31. Veraart J, Poot DH, Van Hecke W, Blockx I, Van der Linden A, Verhoye M, Sijbers J (2011) More accurate estimation of diffusion tensor parameters using diffusion Kurtosis imaging. Magn Reson Med Off J Soc Magn Reson Med Soc Magn Reson Med 65(1): 138–145. doi:10.1002/mrm.22603

32. Lazar M, Jensen JH, Xuan L, Helpern JA (2008) Estimation of the orientation distribution function from diffusional kurtosis imaging. Magn Reson Med Off J Soc Magn Reson Med Soc Magn Reson Med 60(4):774–781. doi:10.1002/mrm.21725

33. Douaud G, Behrens TE, Poupon C, Cointepas Y, Jbabdi S, Gaura V, Golestani N, Krystkowiak P, Verny C, Damier P, Bachoud-Levi AC, Hantraye P, Remy P (2009) In vivo evidence for the selective subcortical degeneration in Huntington's disease. Neuroimage 46(4):958–966. doi:10.1016/j.neuroimage.2009.03.044

34. Douaud G, Jbabdi S, Behrens TE, Menke RA, Gass A, Monsch AU, Rao A, Whitcher B, Kindlmann G, Matthews PM, Smith S (2011) DTI measures in crossing-fibre areas: increased diffusion anisotropy reveals early white matter alteration in MCI and mild Alzheimer's disease. Neuroimage 55(3):880–890. doi:10.1016/j.neuroimage.2010.12.008

35. Jbabdi S, Behrens TE, Smith SM (2010) Crossing fibres in tract-based spatial statistics. Neuroimage 49(1):249–256. doi:10.1016/j.neuroimage.2009.08.039

36. Vos SB, Jones DK, Jeurissen B, Viergever MA, Leemans A (2012) The influence of complex white matter architecture on the mean diffusivity in diffusion tensor MRI of the human brain. Neuroimage 59(3):2208–2216. doi:10.1016/j.neuroimage.2011.09.086

37. Wheeler-Kingshott CA, Cercignani M (2009) About "axial" and "radial" diffusivities. Magn Reson Med Off J Soc Magn Reson Med Soc Magn Reson Med 61(5):1255–1260. doi:10.1002/mrm.21965